

Mapping H₂ Excitation and Mass across NGC 5194 with the Spitzer IRS

Gregory Brunner^{1,2}

Department of Physics and Astronomy, Rice University,
Houston, TX 77005

gbrunner@ipac.caltech.edu, gbrunner@rice.edu

Kartik Sheth³, Lee Armus³, and George Helou³

Spitzer Science Center, Pasadena, CA 91125

Eva Schinnerer⁴

Max-Planck-Institüt für Astronomie, Heidelberg, Germany

and

Stuart Vogel⁵ and Mark Wolfire⁵

Department of Astronomy, University of Maryland, College Park, MD 20741

Received _____; accepted _____

¹Department of Physics and Astronomy, Rice University, Houston, TX 77005

²Visiting Graduate Student Fellow, Spitzer Science Center, Caltech, Pasadena, CA

³Spitzer Science Center, Caltech, Pasadena, CA

⁴Max-Planck-Institüt für Astronomie, Heidelberg, Germany

⁵Department of Astronomy, University of Maryland, College Park, MD

ABSTRACT

We have mapped H₂ pure rotational line emission for the H₂ S(0), H₂ S(1), H₂ S(2), H₂ S(3), H₂ S(4), and H₂ S(5) lines over a strip across NGC 5194 using the *Spitzer Space Telescope* Infrared Spectrograph low resolution modules. The H₂ line intensity maps reveal differences in the molecular gas morphology of NGC 5194. We use the H₂ maps to examine the H₂ excitation-temperature and mass across the galaxy. We find that within our beam, H₂ exists in a continuous distribution of temperatures across the galaxy. We measure the H₂ excitation-temperature of both the "warm" (T = 100 - 300 K) and "hot" (T = 400 - 1200 K) mass distributions traced by the H₂ S(0) - H₂ S(2) and H₂ S(2) - H₂ S(5) lines, respectively. We investigate the origin of the H₂ emission by comparing the location of H₂ emission and mass to photodissociation regions (traced by CO), shock-excited [O IV](25.89 μ m) emission, and X-ray dissociation regions from *Chandra* observations. We find that within the spiral arms, the H₂ mass correlates with the CO (J = 1 - 0) emission; although, we see offsets in the location of the peaks in H₂ mass and CO intensity. Comparing H₂ line intensity to CO intensity reveals that within the spiral arms, pure rotational H₂ line emission is generally cospatial with CO emission indicating that the pure rotational H₂ line emission is originating from the surface layers of dense molecular clouds associated with star-forming regions. Within the nuclear regions of NGC 5194, the hot H₂ phase is copatial with [O IV](25.89 μ m) emission and X-ray emission while the warm H₂ is not. Comparison between the X-ray emission and H₂ line emission reveal that the H₂ morphology is correlated with the X-ray morphology.

Subject headings: galaxies: ISM — galaxies: H₂ — galaxies: individual(NGC 5194)

1. Introduction

Star formation and galactic evolution are inherently connected with molecular hydrogen (H_2) within a galaxy. In the Milky Way, all star formation occurs in molecular clouds (Blitz 1995); although, not all molecular clouds are actively forming stars. In galaxies, star formation is triggered whenever the molecular gas surface density is enhanced, for example, by a spiral density wave (Vogel et al. 1988), by increased pressure as in galactic nuclei (Young and Devereux 1991), due to the hydrodynamic shock along the leading edge of bars, and in the transition region at the ends of bars (Sheth et al. 2000, Kenney and Lord 1991). Although the connection between star formation and molecular gas is well-established, the exact mechanisms for initiating, controlling, and inhibiting star formation are not well-known.

The Whirlpool Galaxy (M51a, NGC 5194) is a nearby, face-on galaxy that has been extensively studied in X-rays (Palumbo et al. 1985, Terashima et al. 2001); UV, optical (Scoville et al. 2001), and IR (Calzetti et al. 2005); submillimeter (Matsushita et al. 2004); millimeter (Helper and Blitz 1997); and radio wavelengths (Murphy et al. 2005). At a distance of 9.6 Mpc (Sandage and Tammann, 1975), its proximity, orientation, and morphology make it an ideal target for studies of the interstellar medium (ISM) across distinct dynamical, chemical, and physical environments in a galaxy. Studies have revealed variations in CO emission and UV radiation field, metallicity gradients, and temperature across the galaxy. Thus, it has been called a *Rosetta Stone* for galaxy evolution (Scoville and Young, 1983).

The Spitzer Space Telescope Infrared Spectrograph (IRS) (Houck et al. 2004) is a powerful tool for observing the H_2 within galaxies and thus deciphering the evolution of M51a. The Spitzer IRS low resolution modules cover 5 - 38 μm (SL, 5 - 14 μm ; LL, 14 - 38 μm) giving observers access to the lowest pure rotational lines of H_2 . These lines trace the

warm ($T = 100 - 1000\text{K}$) molecular gas and are important diagnostics of the ISM allowing for the determination of the H_2 excitation-temperature, mass, and ortho-to-para ratio of H_2 . Thus, by understanding the pure rotational H_2 line emission from a galaxy, constraints can be placed on the energy injection mechanisms (i.e. radiative heating, shocks, turbulence) that heat the molecular gas phases in the ISM.

In this paper, we present spatially resolved observations of the H_2 rotational lines across a radial strip of NGC 5194. Using the Spitzer IRS, we have spectrally mapped a radial strip ($295'' \times 51''$ in the long low module and $324'' \times 57''$ in the short low module) across NGC 5194 in order to understand the conditions of the warm ($T = 100 - 1000\text{ K}$) molecular ISM across dynamically distinct environments. From the spatially resolved IRS low resolution spectra, maps of emission from the six lowest pure rotational transitions of H_2 , the $\text{H}_2(0-0)\text{S}(0)$ ($28.22\text{ }\mu\text{m}$), $\text{H}_2(0-0)\text{S}(1)$ ($17.04\text{ }\mu\text{m}$), $\text{H}_2(0-0)\text{S}(2)$ ($12.28\text{ }\mu\text{m}$), $\text{H}_2(0-0)\text{S}(3)$ ($9.66\text{ }\mu\text{m}$), $\text{H}_2(0-0)\text{S}(4)$ ($8.02\text{ }\mu\text{m}$), and $\text{H}_2(0-0)\text{S}(5)$ ($6.91\text{ }\mu\text{m}$) lines were created. These maps represent measurements of extinction corrected line flux across NGC 5194 (presented in §3.1). Maps are used to determine the spatial distribution of the H_2 excitation-temperature and mass across the galaxy (§3.2). The dominant excitation mechanism of H_2 (photodissociation by UV photons, shocks, and/or x-ray dissociation) is determined in various regions across the galaxy by comparing the H_2 distribution to CO ($J = 1 - 0$) emission (§4.2), [OIV] ($25.89\text{ }\mu\text{m}$) emission (§4.3), and x-ray emission (§4.4).

2. Observations and Data Reduction

2.1. Spectral Data

Spectra were obtained for NGC 5194 using the two low-resolution modules of the Infrared Spectrograph in spectral mapping mode. In spectral mapping mode, we moved the

IRS in a series of discrete steps settling at each position before beginning integration. Half slit spacing were used for all integrations. Integration times in the SL and LL were 14.6 s. Each slit position was covered twice. In total, 1,412 spectra were taken in the SL while 100 were taken in the LL (including background observations). SL integrations were taken perpendicular to the LL integrations in accordance with the SINGS radial strip mapping strategy specified in by Kennicutt et al. (2003). Further details on the observation strategy are available on SST’s Leopard for project ID 200138 (PI: K. Sheth). Dedicated off source background observations were taken for the SL observations. Backgrounds for the LL observations were taken from outrigger data collected while the spacecraft was mapping in the adjacent module.

The spectra were assembled from the basic calibration data into spectral cubes for each module using CUBISM (Smith et al. 2007, in preparation). CUBISM allows for the assembly of cubes, extraction of spectra, and creation of spectral maps. Background subtraction and bad pixel removal was done within CUBISM. The individual IRS spectra were processed using version S14.0 of the Spitzer Science Center pipeline.

In CUBISM, the SL and LL data cubes have resolutions of $1.85''/\text{pixel}$ and $5.08''/\text{pixel}$. The spatial resolution of the data cubes varies as a function of wavelength due to a wavelength dependent point spread function (PSF). Though the pixels are square, the PSF is circular and expands in radius with increasing wavelength. Thus, we define the spatial resolution at a given wavelength in the SL and LL data cubes as

$$R_{SL}(\lambda) = 1''.85 * \lambda / 5.2\mu\text{m} \quad (1)$$

and

$$R_{LL}(\lambda) = 5''.08 * \lambda / 14.0\mu\text{m}, \quad (2)$$

respectively, where λ is the wavelength.

Spectral maps of the H₂S(0) - H₂S(5) lines were created with PAHFIT (Smith et al. 2007), a robust mid-infrared spectral fitting routine. PAHFIT decomposes an IRS low resolution spectrum allowing the recovery of the full flux of blended features. This allows the recovery of the full line flux of the H₂ features, including severely blended lines such as H₂S(1), blended with the 17 μm PAH complex (Smith et al. 2004); H₂S(2), blended with [NeII](12.8 μm); and H₂S(5), blended into [ArII](6.9 μm).

In order to run PAHFIT through the SL and LL data cubes, the grid of the SL1 data cube was interpolated to the grid of the SL2 data cube. The data cubes were then concatenated into one SL cube. The same procedure was used to concatenate the LL1 and LL2 data cubes into one LL data cube. In regions where the first order (SL1, LL1) spectra overlapped with the second order (SL2, LL2) spectra, the first order spectra were scaled up to the second order spectra. The concatenated data cubes were then smoothed spatially by a 3 x 3 pixel box to increase the signal to noise ratio of spectra. Grouping spectra was also done to avoid pixel aliasing, which has the affect of creating a saw-tooth pattern in the continuum (CUBISM User Manual). PAHFIT was then run through both the SL and LL data cubes. The SL data cube was fit separately from the LL data cube.

PAHFIT decomposes every spectrum in both the SL and LL data cubes. In doing so, PAHFIT returns fit parameters to the specified features in the spectrum. These parameters include extinction-corrected integrated line flux, line FWHM, line equivalent width, and uncertainty. The integrated flux measurements are extinction corrected within PAHFIT (see Smith et al. 2007 for the extinction curve). While running PAHFIT through the data cubes, information concerning the position of each spectrum was retained. This allows for the reconstruction of spectral feature (PAH, H₂, ionization line) maps from the results of PAHFIT. When using PAHFIT on an entire data cube, maps of every feature specified by PAHFIT were returned. Additionally, the fit to each spectrum was retained and the fit to

the continuum was reconstructed from internal PAHFIT functions. From these two data cubes, a residual data cube and a continuum subtracted data cube were created for both the SL and LL data cubes. These data cubes are crucial in determining the consistency of the fitted spectra. In order to check the accuracy of the map of H₂S(3) integrated flux, it was compared it to the image created from the continuum subtraction to the SL data cube.

In using PAHFIT, the default values for the temperatures of the starlight and eight thermal dust continuum components were used to fit the continuum. Additionally, the optical depth of the dust extinction at 9.7 μm and 18 μm were also fit. This was especially important in recovering an accurate measurement of the H₂S(3) 9.6 μm line in the 9.7 μm silicate absorption trough.

2.2. CO Map

The BIMA (Berkely Illinois Maryland Array) CO (J=1-0) map was acquired as a part of the BIMA Survey of Nearby Galaxies (SONG) (Regan et al. 2001; Helfer et al. 2003). The CO map was mosaicked from 26 fields. The beam size is 5.8 x 5.1 arcsec (220 x 190 pc), the velocity channel width is 10 km s⁻¹, and the root-mean-square (rms) noise level is 61 mJy beam⁻¹.

2.3. X-ray Emission

The map of x-ray emission from M51 was observed by the Advanced CCD Imaging Spectrometer (ACIS) on the *Chandra X – Ray Observatory* on 20 June 2000. The total integration time was 14,865 seconds. Further details of the observations are presented in Terashima and Wilson (2001).

3. Results

3.1. H₂ Emission Maps

Molecular Hydrogen emission has been detected across NGC 5194. The H₂ S(0), H₂ S(1), H₂ S(2), H₂ S(3), H₂ S(4), and H₂ S(5) lines have been mapped across the radial strip. In figures 1 and 2, maps of the extinction corrected flux of the H₂ S(0) - H₂ S(5) lines are presented. The H₂S(0) and H₂S(1) lines (figure 1) lie in the LL module of the IRS and the resolution of the maps are 10".2 and 6".17, respectively. The H₂ S(2), H₂ S(3), H₂ S(4), and H₂ S(5) lines (figure 2) lie in the SL module of the IRS and these maps have spatial resolutions of 4".37, 3'.44, 2".85, and 2".46, respectively. The differences in resolution between the H₂ maps explains the relative smoothness of H₂S(0) and H₂S(1) maps compared to the H₂S(2) - H₂S(5) maps. Table 2 lists the resolution of the maps. The boxes around the maps represent the regions over which the lines were mapped.

Maps reveal remarkable differences in the morphology of NGC 5194. H₂S(0) emission is strongest in the NW spiral arm with much lower levels of emission coming from the nucleus. The H₂S(1) emission peaks in the nucleus of the galaxy with strong emission in the NW and SE spiral arms. In the H₂S(0) and H₂S(1) emission, we are able to resolve molecular hydrogen emission in the outer spiral arms at several kiloparsecs from the center of the galaxy. While we have resolved molecular hydrogen emission in the outer spiral arms, the peaks in H₂S(0) and H₂S(1) emission within the arms do not align.

The higher resolution H₂S(2) - H₂S(5) maps also show different morphology to NGC 5194. The H₂S(2) map shows the strongest emission in the nuclear region of NGC 5194. The H₂S(3) line exhibits similar strong emission in the nuclear region; however, there appears to be a bar structure across the nucleus of the galaxy going north-to-south. Again, we see offsets in the peak emission within the spiral arms of NGC 5194. These offsets are

real and indicate variations in the excitation-temperature in each region.

Maps of the H₂S(4) and H₂S(5) lines show a remarkably different morphology to the nuclear region of NGC 5194. The H₂S(5) nuclear emission follows the nuclear emission of the H₂S(3) line, while the H₂S(4) nuclear emission mirrors the H₂S(2) emission. This indicates variations in the excitation-temperature (further explored in section §3.3).

Due to the sensitivity of the IRS low resolution module, we were unable to resolve H₂S(4) and H₂S(5) emission beyond the central region of NGC 5194. For the same reason, we were unable to create maps of the H₂S(6) (at 6.11 μ m) and H₂S(7) (at 5.51 μ m) lines. Deeper observations could reveal more complete maps of the H₂S(4) and H₂S(5) emission in NGC 5194 in addition to allowing us to map the H₂S(6) and H₂S(7) lines across NGC 5194.

4. Discussion

4.1. H₂ Excitation-Temperature and Mass across NGC 5194

The pure rotational lines of molecular hydrogen provide a powerful probe of the conditions of the ISM and place constraints on the energy injection processes that excite H₂. Knowledge of the extinction corrected flux of the H₂S(0) - H₂S(5) lines allow for the mapping of the excitation-temperature and number density (and consequently mass). The excitation-temperature and mass can be modeled across the galaxy by creating excitation diagrams at every position across the strip of NGC 5194.

Excitation diagrams across NGC 5194 were created from the maps of H₂ emission. Each map was smoothed and interpolated to the resolution of the H₂S(0) line. The non-rectangular shape to the excitation-temperature and mass are due to the offset in alignment between the LL and SL strips. Excitation diagrams across the strip were derived

from the Boltzman equation in similar form to the Rigopoulou et al. (2002).

$$N_i/N = (g(i)/Z(T_{\text{ex}})) \exp(-T_i/T_{\text{ex}}) \quad (3)$$

where $g(i)$ is the statistical weight of state i , $Z(T_{\text{ex}})$ is the partition function, T_i is the energy level of a given state, and T_{ex} is the excitation temperature. N and N_i are the total column density and the column density of a given state i and is determined directly from the measured extinction corrected flux by

$$N_i = \text{flux}(i)/(A(i)h\nu(i)) \quad (4)$$

where $A(i)$ and $\nu(i)$ are the A-coefficient and frequency of state i and h is Planck's constant. Table 1 lists the values for the wavelength ($\lambda(i)$), rotational state (J), $A(i)$, T_i , and $g(i)$ of the pure rotational levels of H_2 that lie in the wavelength range covered by the IRS low resolution modules.

The excitation diagrams exhibit an ortho-to-para ratio (OPR) in the nuclear region 3 (in agreement with the value of the OPR of the nuclear region determined by SINGS (Roussel et al. 2007, in press); this is determined from the fit to the best two-component fit to the $H_2S(0)$ - $H_2 S(5)$ lines. Outside of the nuclear region, poor detection of the $H_2 S(4)$ and $H_2 S(5)$ lines prevents the mapping of OPR across the disk; however, the lower J lines exhibit an OPR of 3 within the spiral arms.

In the nuclear region of NGC 5194, the excitation diagram is smooth and its slope decreases at higher rotational levels (Figure 3). This indicates that there is a range of temperatures being sampled within the beam. Similar behavior has been observed in extragalactic targets by surveys of Seyferts (Rigopoulou et al. 2002) and ULIRGS (Higdon et al. 2006). The temperature of the warm ($T = 100$ - 300 K) H_2 and the temperature of the hot ($T = 400$ - 1200 K) H_2 can be determined from the excitation diagrams by fitting the $H_2S(0)$ - $H_2S(2)$ lines and the $H_2S(2)$ - $H_2S(5)$ lines respectively (as opposed to fitting all of the observed H_2 rotational lines in order to derive a temperature of the warm H_2).

From a two-component fit to the excitation diagram, the excitation-temperature of the “warm” and “hot” components of H₂, the “warm” and “hot” H₂ mass have been mapped across NGC 5194 (figures 4, 5, and 6). In measuring the mass in H₂, we determine the mass from the number density by multiplying the column density by the physical area within the beam (Rigopoulou et al. 2002). At 9.6 Mpc (Sandage and Tammann 1975), 5.08 arcsec corresponds to 236.43 parsecs. The maps of the mass distribution are in units of solar masses within a 55.899 kpc² region.

Figure 4 compares the warm H₂ mass to the temperature distribution of the mass. The gas is warmest in the central region of NGC 5194 with the temperature ranging from 225K - 275 K in the center of the galaxy. The gas is coolest within the spiral arms of NGC 5194. The outer NW and SE spiral arms (at about 6-7 kpc from the center of the galaxy each) contain on the order of 10,000 M_⊙ (within a 55.9 kpc² region) and 6,000 M_⊙ (within a 55.9 kpc² region) of H₂ (in the NW and SE arms, respectively) and the gas within the outer spiral arms ranges from 150 K at the center of the arms to about 225 K near the edges. Within the central 000 pc² of the galaxy, there is 000 M_⊙ of warm H₂ and 00000 M_⊙ hot H₂. These values are consistent with the masses of H₂ found in the central regions of Seyferts (Rigopoulou et al. 2002). In NGC 5194, the IRS is sensitive to 375 M_⊙ warm H₂ and 5 M_⊙ hot H₂ within the beam (though the sensitivity to the hot H₂ could be underestimated due to smoothing the H₂S(2), H₂S(3), H₂S(4), and H₂S(5) lines by a factor of 3 times their resolution).

Note that due to zero detection of H₂ in some of the inner arm regions, we are unable to determine the temperature distribution across the entire strip. This is evident towards the NW and SE edges of the radial strip.

The temperature and mass distribution of the hot H₂ reveals a different picture (Figure 5). There is significantly less mass in the hot H₂ phase, on the order several hundred M_⊙,

depending on the region. The greatest amount of hot H₂ is found within the nuclear region of NGC 5194; this is much different from the warm H₂ that dominates the spiral arms. The hot gas exhibits cooler temperatures within the central regions of NGC 5194 and the spiral arms. Temperatures are greater in the inter-arm regions where there is less H₂.

Due to the weakness of the H₂S(2), H₂S(3), H₂S(4), and H₂S(5) features beyond the spiral arms, the hot H₂ excitation temperature and mass can not be mapped over the whole strip. While the radial strip across NGC 5194 is helpful in understanding the H₂ excitation-temperature and mass across the disk of the galaxy, complete IRS low resolution coverage of NGC 5194 with longer integration time is necessary in order to understand hot H₂ distribution and the H₂ OPR across the whole galaxy.

4.2. Distinguishing the H₂ Excitation Mechanisms

Previous studies of pure rotational H₂ emission in galaxies have used aperture average spectra over the central regions of galaxies to understand the distribution of the warm and hot molecular gas phases within a galaxy (Rigopoulou et al. 2002, Higdon et al. 2006, Roussel et al. 2007, in press). These studies use the pure rotational lines to derive excitation-temperatures and warm and hot H₂ masses of the H₂ within the galaxy. Additionally, these studies compare the warm and hot H₂ mass to the cold H₂ mass traced by CO emission to in order to understand the mass fractions of the cold (T = 5 - 10 K), warm, and hot H₂ mass. These studies have had difficulty distinguishing the H₂ excitation mechanisms within the galaxies

H₂ is generally excited via three processes: 1.) excitation in photodissociation regions (PDRs) , 2.) shocks, and 3.)x-ray dissociation (XDRs). Mapping the warm and hot H₂ mass-excitation temperature and mass distributions provide the information necessary

to understand whether the warm and hot H₂ phases undergo excitation via the same mechanism. This information coupled with spatially resolved diagnostics of PDRs, shocks, and XDRs put constraints on the dominant H₂ excitation mechanism in NGC 5194, in different regions within NGC 5194.

Figure (??) compares the warm H₂ excitation temperature distribution to the mass distribution. The excitation temperature is greatest within the nuclear region of the galaxy and is cooler in the spiral arms. Within the nuclear region, the excitation temperature decreases moving radially away from the center of the galaxy. Moving into the inner spiral arms, the excitation temperature decreases. The excitation temperature within the inter-arm regions is greater than in the spiral arms.

The excitation-temperature for the hot H₂ phase peaks in the inter-arm regions (figure ??); the hot H₂ mass peaks in the nuclear region of the galaxy. This is contrasted to the warm H₂ mass that peaks in the SW spiral arm. Directly comparing the warm H₂ mass to the hot H₂ mass, shows that the ratio of warm-to-hot H₂ is greater in spiral arms than in the nuclear region of the galaxy (figure ??). In the nuclear region of the galaxy, the ratio of warm-to-hot H₂ is 100. Moving into the NW inner spiral arm and SE inner spiral arm, the ratio increase by a factor of 8 and 6.5 respectively.

The variations of the warm-to-hot mass ratio across the strip over NGC 5194 indicates that the primary excitation mechanisms of the warm and hot H₂ differ. The warm H₂ mass peaks in the NW inner spiral arm whereas the hot H₂ mass peaks in the center. This suggests that the warm H₂ is associated with giant molecular clouds within spiral arms and is primarily excited by PDRs. NGC 5194 is known to host a weak AGN in its nucleus (citation). The hot H₂ mass peaks in the nuclear region. This could mean that the warm phase is primarily excited by the AGN.

In order to understand the excitation mechanisms of the warm H₂ and the hot H₂

and where each is dominant, we present comparisons of the H₂ mass distributions to diagnostics of the three excitation mechanisms (PDRs, shocks, and XDRs). CO rotational transitions are used as diagnostic lines of PDRs (Allen et al., 2004). Comparing the H₂ mass distributions to CO ($J = 1 - 0$) thus compares the location of the H₂ mass to locations of giant molecular clouds. The [OIV](25.98 μm) emission arises from shocks (Schaefer and Stasinska 1999). Spatial mapping of [OIV](25.89 μm) emission thus serves to discern regions where H₂ is excited primarily by shocks. H₂ excitation by x-rays can also be discerned within M51a by comparing the H₂ mass phases and emission to x-ray emission observed by the Chandra X-ray Observatory (Terashima and Wilson 2001). The following sections compare the H₂ mass distributions to CO ($J = 1 - 0$) emission, [OIV](25.89 μm) emission, and x-ray emission.

4.3. H₂ Excitation by PDRs: Comparison of H₂ to CO emission

Within a molecular cloud, H₂ exists from the interface between the HII region and PDR front, deep into the PDR. Owing to an ionization potential of 4.5 eV, H₂ formation generally does not occur within a PDR until the radiation field becomes sufficiently weak. The H₂ -PDR connection has become the emphasis of many theoretical models recently. Recent advances in the CLOUDY photoionization modeling code have included H₂ and modeled the structure of star forming regions while treating the HII region and PDR as one continuous cloud (Shaw et al. 2005, Abel et al. 2005). Kaufman et al. (2006) examined H₂ pure rotational line emission from PDRs to probe the conditions of dense PDRs in star forming regions. They show that within galaxies, where the telescope beam size is generally kiloparsecs across, H₂ emission could serve to probe the surface layers of dense molecular clouds.

CO emission arises from deep within a molecular cloud where the temperatures are too

cold to excite H₂ emission. In these regions, CO is collisionally excited by the much more abundant H₂ molecule. Thus, molecular gas within molecular clouds has generally been studied via observations of CO rotational line emission. Here, we compare the warm and hot H₂ mass phases and H₂ rotational line emission to CO ($J = 1 - 0$) emission (mapped by BIMA SONG) in order to understand the relationship between H₂ emission and PDRs.

Figure (??) compares the warm and hot H₂ mass distributions to CO emission. Within the spiral arms, the H₂ mass is generally aligned with CO emission; however, there are offsets in the location of the peaks in the H₂ mass and CO emission. This is real and is not due to the difference in resolution between the CO map ($6''$) and the H₂ maps ($10''$). In the NW inner spiral arm, the peak in warm H₂ mass is offset to the NW of the peak in CO emission. At even larger distances from the nucleus of NGC 5194, we observe the H₂ mass offset from the CO emission within the outer NW spiral arm. In this case, the H₂ mass is offset to the SE of the CO emission. Additionally, in the SE outer spiral we observe H₂ in a region that appears devoid of CO emission. These regions where the peaks are offset or there is not CO emission where H₂ is observed could just be spiral arms that are rich in H₂ but devoid of CO.

Comparing the hot H₂ mass phase to CO emission (Figure ??), the hot H₂ mass peaks in the nuclear region while the CO emission peaks in the spiral arms. In the NW and SE spiral arms, the CO emission is found within the wider H₂ mass contours. This is a result of the difference in resolution between the H₂ maps ($10''$) and the BIMA SONG CO map ($6''$).

Figure (??) compares the CO emission to the H₂ rotational line emission for H₂ S(0), H₂ S(1), H₂ S(2), and H₂ S(3). These maps all resolve H₂ emission within the nucleus and spiral arms of the galaxy. The H₂ S(2) and H₂ S(3) maps (at resolutions of $3''.44$ and $4''.37$, respectively) show strong correlation between H₂ and CO emission within the spiral

arms. In the spiral arms, the H₂ emission generally traces the CO emission with the one exception that in the H₂ S(2) map, H₂ emission in the SE spiral arm is offset to the SE by 2" from the CO spiral arm. Comparing the H₂ S(1) map to CO emission shows that a strong correlation between H₂ and CO emission in the spiral arms. In this case both maps are at similar resolutions (~ 6") and the H₂ contours trace the CO emission (though it should be noted that the H₂ contours appear wider than the CO emission; this is an effect of grouping spectra prior to fitting). The comparison between the H₂ S(0) and CO emission shows that the H₂ S(0) and CO emission are correlated; however, we notice offsets in the emission peaks for CO and H₂ S(0).

While H₂ rotational line emission and CO are correlated in the spiral arms, the peaks in H₂ S(2) and H₂ S(3) emission both occur in the nucleus of NGC 5194. Within the H₂ S(2) and H₂ S(3) emission peaks, the CO emission is offset to the north of the H₂ intensity peaks. This suggests that while H₂ emission is excited within PDRs associated with dense molecular clouds in the spiral arms, a different process is the dominant excitation mechanism of the higher J lines and the hot H₂ phase within the nuclear region of NGC 5194.

4.4. H₂ Excitation by Shocks: Comparison of H₂ to [OIV](25.89 μm) emission

The [O IV](25.89 μm) line can be excited in shocks, the stellar winds of massive Wolf-Rayet stars, or by a active galactic nucleus (AGN)(Schaerer and Stasinska 1999, Lutz et al. 1998, Smtih et al. 2004). Though the [O IV](25.89 μm) line is bledened with the [Fe II](25.99 μm) line in Spitzer IRS low resolution spectra, PAHFIT can deblend the two lines. Thus, in mapping the H₂ S(0) and H₂ S(1) line in the LL data cubes, [O IV](25.89 μm) emission was also be mapped at a resolution of 9".39 ($\lambda/\delta\lambda = 142$). Figure (??) compares the [O IV](25.89 μm) emission to the hot H₂ disribution. The [O IV](25.89 μm)

map, warm H₂ map, and hot H₂ map all have comparable resolutions (9".39, 10".2, and 10".2, respectively). The [O IV](25.89 μm) emission is brightest in the central region of the galaxy and its peak is cospacial with the peak in the mass of the hot H₂. Moving from the nucleus to the inner spiral arm, the [O IV](25.89 μm) emission subsides. Note also weak [O IV](25.89 μm) emission within the spiral hot H₂ spiral arms and in the inter-arm region (toward the SE spiral arm).

The [O IV](25.89 μm) emission within the nuclear region is likely due to the weak Seyfert 2 nucleus (Ford et al. 1985) and is possibly associated with shocked gas from the outflows of the AGN. The peak of the [O IV](25.89 μm) emission coincides with the peak in hot H₂ mass indicating that the hot H₂ phase in the nuclear region of the galaxy is AGN or shock heated. With about 1000 M_{\odot} of hot H₂ in the central 0.5 kpc², it is unlikely that the hot H₂ is fueling the central AGN, but rather is excited by the AGN or shocks produced by it. In the nuclear region we observe a factor of 100 times greater warm H₂ mass in the nucleus. While there is significantly more mass in the warm phase, the warm H₂ mass is much greater within the spiral arms than within the nucleus. Thus, the warm H₂ is not primarily excited by shocks.

4.5. H₂ Excitation by XDRs: Comparison of H₂ to X-ray emission

M51 has been extensively studied in x-rays by ASCA (Terashima et al. 1998), Newton XMM (Dewangen et al. 2005), and the Chandra X-ray Observatory (Terashima and Wilson 2001). These observations of the M51a,b system have revealed more than 80 x-ray sources. Candidates for these x-ray sources include neutron stars, black holes, supernova remnants (SN 1994I), and a low-luminosity AGN (Terashima et al. 2006, Immler et al. 2002, Terashima and Wilson 2001). X-ray emission from the nuclear region of NGC 5194 has been studied by Terashima and Wilson (2001). At 1" resolution, they observe x-ray

emission from the nucleus, an extranuclear cloud (XNC, to the south of the nucleus), and the northern loop. A radio jet has been observed connecting the nucleus of NGC 5194 to the XNC in 6 cm imagery (Crane and van der Hulst 1992). The jet emanates from the south of the elongated nucleus and is shock heating ISM.

Figure (?) compares the 0.5 - 10 keV x-ray band image to the warm and hot H₂ mass distributions. There is very little correlation between the 0.5 - 10 keV x-ray emission and the warm H₂ mass distribution indicating that x-rays play very little role in heating the warm H₂ mass. X-ray emission does correlate with the hot H₂ mass. The brightest 0.5 - 10 keV x-ray emission originates from the nucleus and the southern XNC. The hot H₂ mass peak is cospatial with the nucleus and the mass decreases into the XNC. Additionally, the hot H₂ mass decreases moving into the northern loop. The correlation between x-ray emission from the nucleus of NGC 5194 and the peak in hot H₂ mass suggests that x-rays play an important role in exciting the hot phase of H₂; however, due to the disparity in resolution between the x-ray image and the H₂ maps (1" resolution for x-rays 5".08 resolution for the warm and hot H₂ mass) it is difficult to distinguish between shock excitation and x-ray excitation of H₂ in the nuclear region of NGC 5194.

In order to distinguish between shock excitation and x-ray excitation of H₂ in the nuclear region of NGC 5194, we compare the x-ray emission to the maps of the higher J H₂ emission maps. The H₂ S(2), H₂ S(3), and H₂ S(5) intensity all peak at the X-ray source within the nucleus. The X-ray source fits within the H₂ contours because the X-ray image resolution is better than the resolution of each of the H₂ maps. The morphology of the nuclear H₂ emission is correlated with the X-ray source. The H₂ S(2) intensity peaks around the X-ray nucleus. The intensity decreases to the south and falls off by a factor of 70 % within the southern XNC. The bar structure seen in the H₂ S(3) emission is strongly associated with X-ray emission. The H₂ S(3) intensity peaks between the X-ray nucleus

and the southern XNC. To the north of the nucleus, the contours follow the northern X-ray loop. Additionally, H₂ S(3) intensity decreases by a factor of 80 % from the nucleus to the south of the XNC. Both the H₂ S(4) and H₂ S(5) maps show that the peak in intensity are cospatial with the peaks in X-ray emission.

5. Conclusions

We have spectrally mapped a strip across NGC 5194 using the Spitzer IRS low resolution modules. We used the spatially resolved spectra across to map the lowest pure rotational H₂ lines across the strip. We find:

1. The morphology of H₂ emission in NGC 5194 varies with H₂ rotational level. H₂ S(0) emission is strongest in the spiral arms of the galaxy while the lower J transitions show the strongest emission towards the nucleus. The H₂ S(0) and H₂ S(1) maps (at 10''.2 and 6''.17 resolution, respectively) show emission across the entire strip out to spiral arms located several kpc from the center of the galaxy. The H₂ S(2) and H₂ S(3) maps (at 4''.37 and 3''.44 resolution, respectively) reveal H₂ in the nucleus, spiral arms, and inter-arm regions of NGC 5194 and strong H₂ S(4) and H₂ S(5) emission is resolved in the nuclear region of NGC 5194. The H₂ maps reveal interesting morphology to the molecular gas distributions, such as bar structure across the nucleus in H₂ S(3) emission.
2. The different morphologies of H₂ emission in NGC 5194 indicate variations in H₂ excitation-temperature and mass. From maps of the emission of the lowest pure rotational transitions, the excitation-temperature and mass were mapped across the strip. Excitation diagrams reveal the the H₂ exists in a continuous distribution of temperatures. We used the excitation diagrams to place constraints on the excitation temperature and

masses of the warm ($T = 100 - 300$ K) and hot ($T = 400 - 1000$ K) H₂ mass phases across the NGC 5194 strip coverage.

3. We find that the warm H₂ mass and the hot H₂ mass are not cospatial. The hot mass peaks in the central region of NGC 5194 and the warm mass peaks in the NW spiral arm (in our strip coverage). Direct comparison of the warm and hot H₂ mass phases reveal that the warm-to-hot mass ratio varies across NGC 5194. In the nucleus, the ratio is 100 and it increases to 800 in the NW spiral arm. Variations in the warm-to-hot H₂ ratio and differences in the morphology of the H₂ emission across NGC 5194 indicate that the primary excitation mechanism differs for the warm and hot H₂ mass phases as a function of location within the galaxy.

4. We compared the H₂ mass distributions and the H₂ line intensity maps to the locations of dense PDRs, traced by CO ($J = 1 - 0$) emission. The warm H₂ mass phase aligns with the CO emission within the spiral arms; however, there are offsets in the location of the peaks in H₂ mass and CO emission. We believe that these offsets are real and are possibly associated with regions that are rich in H₂ but devoid of CO. We also compared the H₂ line maps to CO emission intensity. Within the spiral arms, the H₂ is associated with the CO emission indicating that the H₂ emission is most likely associated with the surface layers of dense PDRs.

5. We observed both strong [O IV](25.89 μm) emission and X-ray emission from the nuclear region of the galaxy. The [O IV](25.89 μm) emission and X-ray emission are both cospatial with the hot H₂ mass suggesting that the hot H₂ in the nucleus is primarily excited by the AGN, strong shocks (possibly associated with the central AGN), or X-rays associated with the AGN. We cannot separate the contribution of the excitation

mechanisms due to the 9''.39 resolution of [O IV](25.89 μm) emission map. We compared the X-ray emission in the nuclear region to H₂ S(2), H₂ S(3), H₂ S(4), and H₂ S(5) emission and find that the morphology of these line is correlated with the X-ray emission morphology.

The author graciously acknowledges the Spitzer Science Center Spitzer Visiting Graduate Student Fellowship Program and committee for providing support for this research. The author would like to specifically acknowledge the program coordinators, Phil Appleton and Alberto Noriega-Crepso. The author would also like to thank JD Smith for swift responses to questions about PAHFIT and CUBISM and Nicolas Flagey for productive discussions about PAHFIT.

Facilities: Spitzer Science Center (SSC), Spitzer Space Telescope (SST), Berkely-Illinois-Maryland Array (BIMA).

REFERENCES

- Aalto, S., Hüttemeister, S., Scoville, N.Z., and Thaddeus, P., 1999, AJ, 522, 165
- Abel, N.P., Ferland, G.J., Shaw, G., and van Hoof, P.A.M., 2005, ApJS, 161, 65
- Allen, R.J., Heaton, H.I., and Kaufman M.J., 2004, ApJ, 608, 314
- Blitz, L., 1995, SSR, 684
- Calzetti, D. et al., 2005, ApJ, 633, 871
- Crane, P.C. and van der Hulst, J.M., 1992, AJ, 103, 1146
- Dewangn, G.C., Griffiths, R.E., Choudhury, M., Miyaji, T., and Schurch, N.J., 2005, ApJ, 635, 198
- Ford, H.C., Crane, P.C., Jacoby, G.H., Lawrie, D.G., and van der Hulst, J.M., 1985, ApJ, 293, 132
- Fuente et al., 1999, ApJ, 518, L45 [Helfer and Blitz 1997]hel97 Helfer, T.T. and Blitz, L., 1997,
- Helfer, T.T., Thornley, M.D., Regan, M.W., Wong, T., Sheth, K., Vogel, S.N., Blitz, L., and Bock, D.C.J., 2003, ApJS, 145, 259
- Higdon, S.J.U., Armus, L., Higdon, J.L., Soifer, B.T., and Spoon, H.W.W., 2006, ApJ, 648, 323
- Houck, J.R. et al., 2004, ApJS, 145, 18
- Immler, S., Wilson, A.S., and Terashima, Y., 2002, ApJ, 573, L27
- Kaufman, M.J., Wolfire, M.G., and Hollenbach, D.J., 2006, ApJ, 644, 283

- Lutz, D., Kunze, D., Spoon, H.W.W., and Thornley, M.D., 1998, A&A, 333, L75
- Kennicutt, R.C. et al., 2003, PASP, 115, 928
- kl91 Kenny, J.D.P. and Lord, S.D., 1991, ApJ, 381, 118
- Matsushita, S. et al., 2004, ApJ, 616, L55
- Murphy, E.J. et al., 2006, ApJ, 638, 157
- Neufeld, D.A., Melnick, G.J., and Harwit, M., 1998, ApJ, 506, L75
- Neufeld, D.A., Melnick, G.J., Sonnentrucker, P., Bergin, E.A., Green, J.D., Kim, K.H., Watson, D.M., Forrest, W.J., and Pipher, J.L., 2006, ApJ, 649, 816
- Palumbo, G.G.C., Fabbiano, G., Fransson, C., and Trinchieri, G., 1985, ApJ, 298, 259
- Regan, M.W., Thornley, M.D., Helfer, T.T., Sheth, K., Wong, T., Vogel, S.N., Blitz, L., and Bock, D.C.J., 2001, ApJ, 561, 218
- Rigopoulou, D., Kunze, D., Lutz, D., Genzel, R., and Moorwood, A.F.M., 2002, A&A, 389, 374
- Roussel, H. et al., 2007, in press
- Sandage, A. and Tammann, G.A., 1975, ApJ, 196, 313
- Schaerer, D. and Stasinska, G., 1999, A&A, 345, L17
- Scoville, N.Z. and Young, J.S., 1983, AJ, 265, 148
- Scoville, N.Z., Yun, M.S., Armus, L., and Ford, H., 1998, ApJ, 493, L63
- Scoville, N.Z., Polletta, M., Ewald, S., Stolovy, S.R., Thompson, R., and Rieke, M., 2001, AJ, 122, 3017

Shaw, G., Ferland, G.J., Abel, N.P., Stancil, P.C., and van Hoof, P.A.M., 2005, ApJ, 624, 794

Sheth, K., Regan, M.W., Vogel, S.N., and Teuben, P.J., 2000, ApJ, 532, 221

Sheth, K., Vogel, S.N., Regan, M.W., Thornley, M.D., and Teuben, P.J., 2005, ApJ, 632, 217

Smith, J.D.T. et al., 2004, ApJS, 154, 199

Smith, J.D.T., Armus, L., Buckalew, B., Dale, D.A., Helou, G., Roussel, H., and Sheth, K., 2006, CUBISM User Manual

Smith, J.D.T. et al., 2007, ApJ, 656, 770

Smith, J.D.T. et al., 2007, in press

Sternberg, A. and Neufeld, D.A., 1999, ApJ, 516, 371

Terashima, Y., Ptak, A., Fujimoto, M.I., Kunieda, H., Makishima, K., and Sherlemitsos, P.J., 1998, ApJ, 496, 210

Terashima, Y. and Wilson, A.S., 2001, ApJ, 560, 139

Vogel, S.N., Kulkarni, S.R., and Scoville, S.Z., 1988, Nature, 334, 402

Terashima, Y. and Wilson, A.S., 2001, ApJ, 560, 139

Young, J.S. and Devereux, N.A., 1991, ApJ, 373, 414

Young, J.S. and Scoville, N.Z., 1991, ARA&A, 29, 581

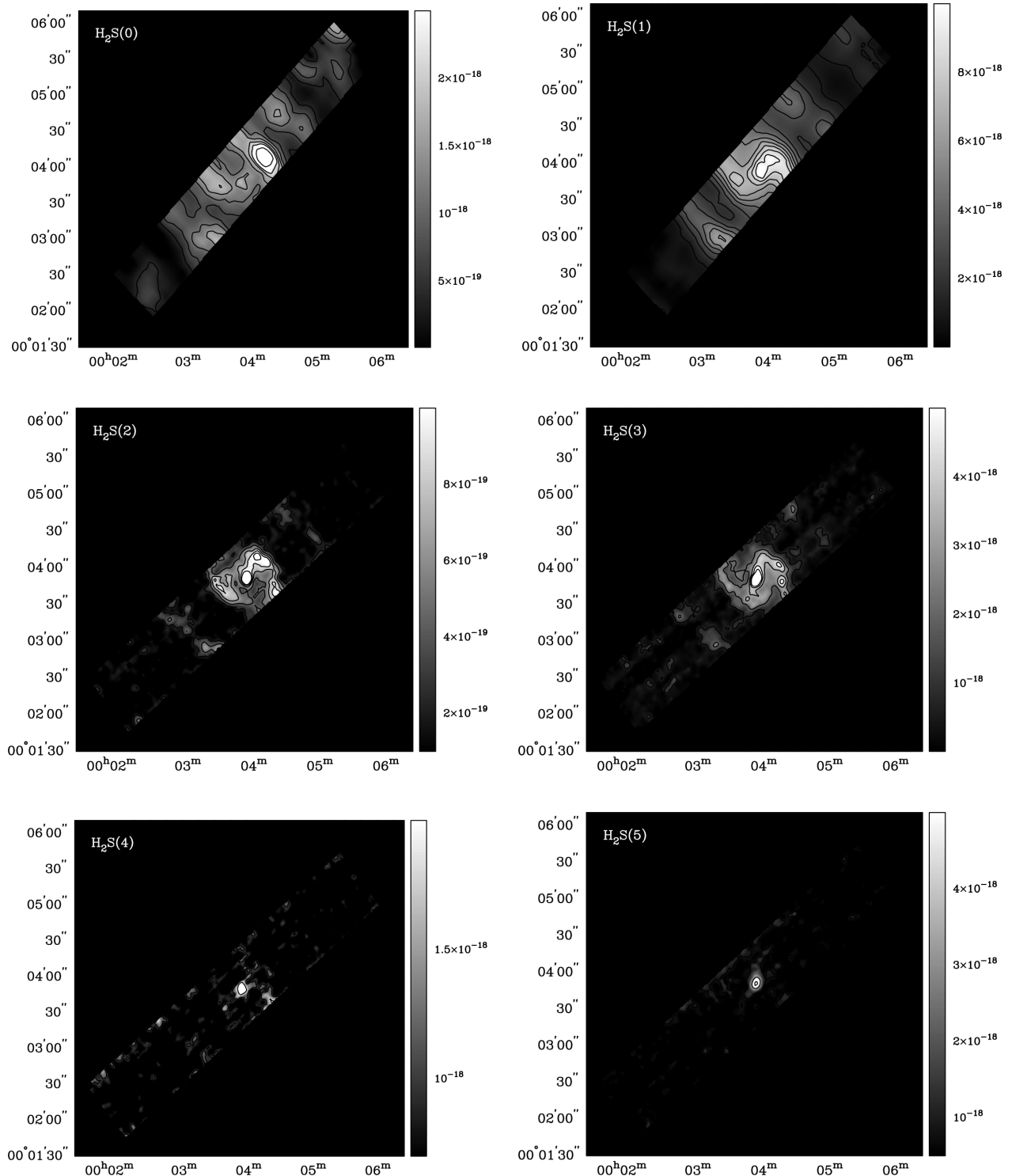


Fig. 1.— Maps of the H₂ S(0) (top left), H₂ S(1) (top right), H₂ S(2) (middle left), H₂ S(3) (middle right), H₂ S(4) (bottom left), and H₂ S(5) (bottom right) emission intensity across the SL and LL strips that were mapped with the Spitzer IRS. The H₂ S(0) and H₂ S(1) maps are created from the LL data cubes. The resolution of the H₂ S(0) and H₂ S(1) maps are 10''.2 and 6''.17, respectively. The H₂ S(2), H₂ S(3), H₂ S(4), and H₂ S(5) maps are created from the SL data cube. The resolution of the H₂ S(2), H₂ S(3), H₂ S(4), and H₂ S(5) maps are 4''.37, 3''.44, 2''.85, and 2''.46, respectively. The grey-scale is in units of W/m². Contour levels are at 2.9×10^{-18} , 2.2×10^{-18} , 1.8×10^{-18} , 1.5×10^{-18} , 1.1×10^{-18} , 7.3×10^{-19} , and 3.7×10^{-19} W/m² for H₂ S(0); 9.6×10^{-18} , 8.6×10^{-18} , 7.5×10^{-18} , 6.4×10^{-18} , 5.4×10^{-18} , 4.3×10^{-18} , 3.2×10^{-18} , 2.1×10^{-18} and 1.1×10^{-18} W/m² for H₂ S(1); 1.1×10^{-18} , 8.9×10^{-19} , 6.7×10^{-19} , 4.4×10^{-19} , and 2.2×10^{-19} W/m² for H₂ S(2); 1.21×10^{-17} , 9.4×10^{-18} , 6.7×10^{-18} , 4.0×10^{-18} , and 1.3×10^{-18} W/m² for H₂ S(3); 2.0×10^{-18} and 1.0×10^{-18} W/m² for H₂ S(4); 7.3×10^{-18} , 4.0×10^{-18} , and 8.0×10^{-19} W/m² for H₂ S(5). The vertical axis is the right ascension and the horizontal axis is the declination. Note that in all of the maps, north is up and west is to the left. The box around the intensity maps represents the SL or LL strip that was mapped.

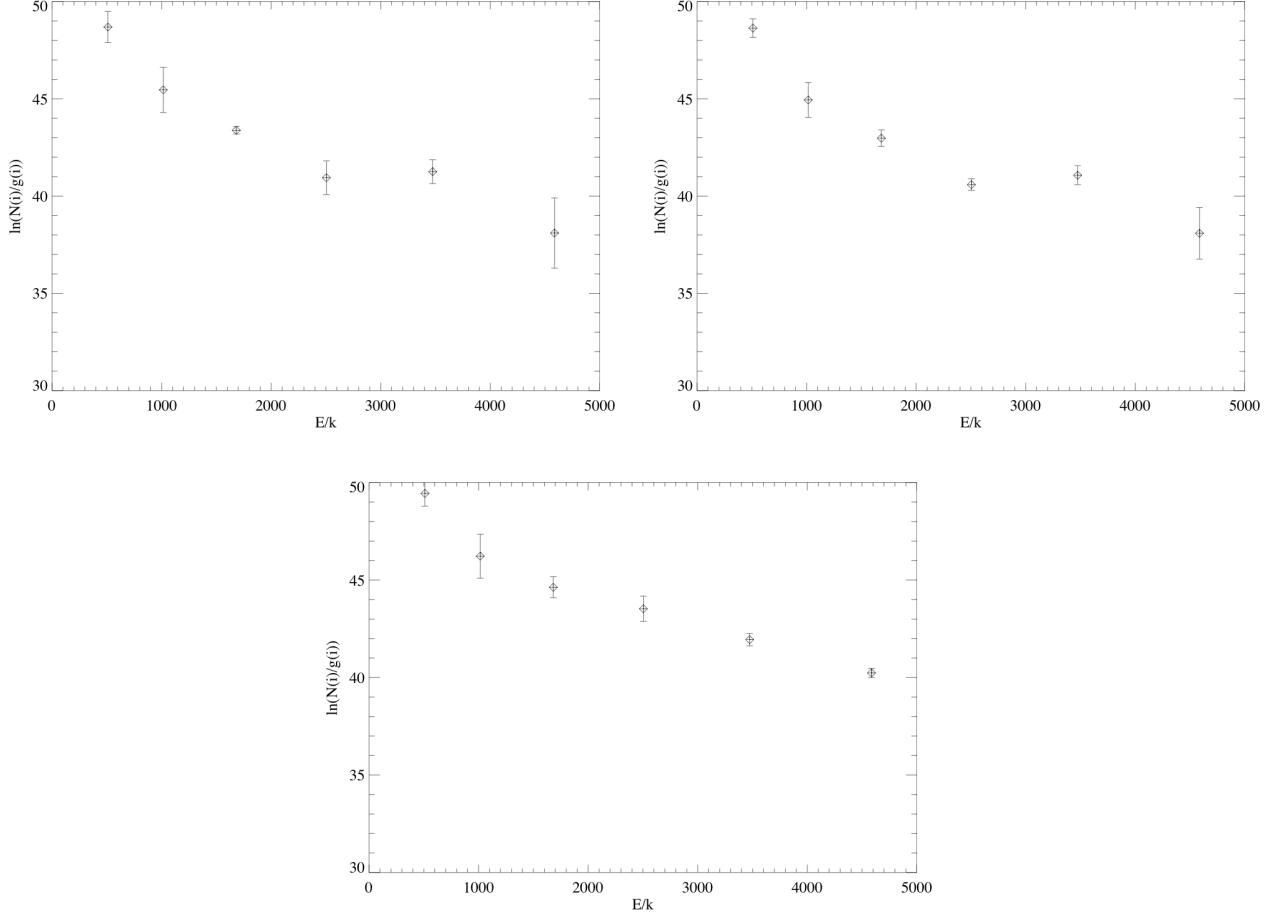


Fig. 2.— Sample excitation diagrams taken from different regions along the NGC 5194 strip. The top two excitation diagrams are taken from the different spiral arms at 25 arcsec^2 regions at (RA, Dec) of (202.45, 47.21) and (202.49, 47.18), respectively. The excitation diagram at the bottom is taken from a 25 arcsec^2 region in the center of NGC 5194 at (RA, Dec) of (202.47, 47.19).

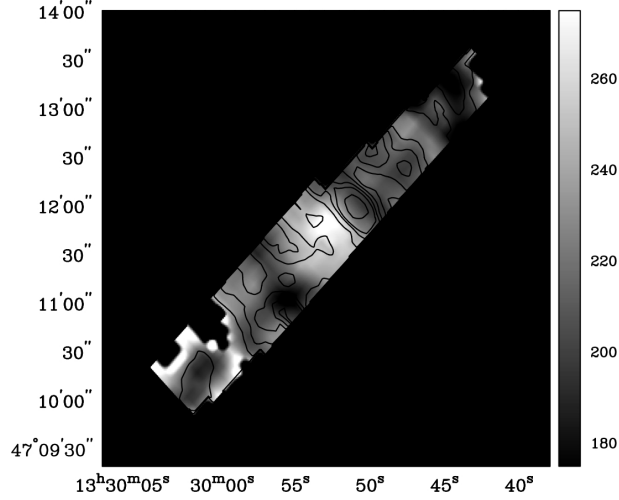


Fig. 3.— The warm ($T = 175 - 275$ K) H_2 mass compared to the warm H_2 excitation-temperature distribution. The warm H_2 excitation-temperature and mass distributions are derived from the fit to the excitation diagrams across the strip for the H_2 S(0), H_2 S(1), and H_2 S(2) lines. Mass density contour levels are 0.45, 0.28, 0.23, 0.17, 0.11, and 0.06 M_\odot/pc^2). Contours represent the mass within a $5.5 \times 10^4 \text{ pc}^2$ area. The grey-scale represents the excitation-temperature distribution (in units of Kelvin). The non-rectangular shape to the map is due to the slight offset of the Spitzer IRS SL strip relative to the LL strip.

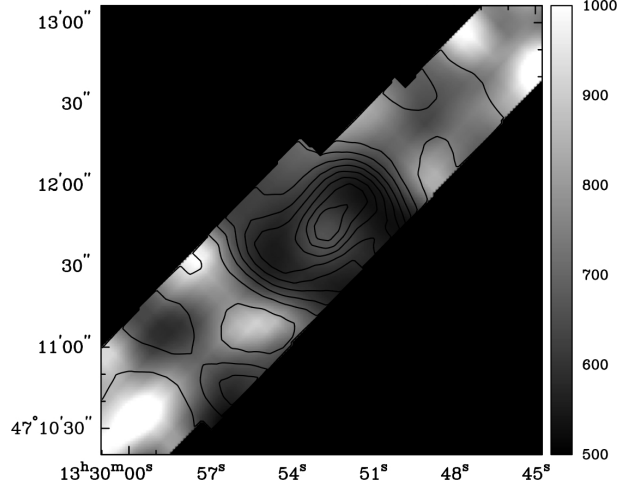


Fig. 4.— The hot ($T = 500 - 1000$ K) H_2 mass compared to the hot H_2 excitation-temperature distribution. The hot H_2 excitation-temperature and mass distributions are derived from the fit to the excitation diagrams across the strip for the H_2 S(2), H_2 S(3), H_2 S(4), and H_2 S(5) lines. Mass density contour levels are at 10% of the maximum mass density ($0.002 M_\odot/\text{pc}^2$). Contours represent the amount of mass of the hot H_2 within a $5.5 \times 10^4 \text{ pc}^2$ area. The grey-scale represents the excitation-temperature distribution (in units of Kelvin). Note that the due to lack of H_2 detection from the higher J lines a greater distances from the nucleus of NGC 5194, we are unable to map the hot H_2 distributions across the entire strip as we have done for the warm H_2 distribution.

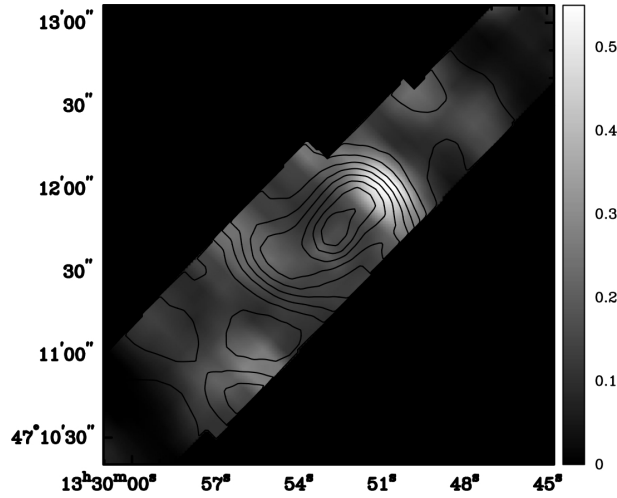


Fig. 5.— The warm (175K - 275 K) H₂ mass (in grey-scale) compared to the hot (T = 500 - 1000 K) H₂ mass (in contours). Contours levels for the hot H₂ mass distribution are at 10% of the maximum mass density ($0.002 M_{\odot}/pc^2$). Contours represent the amount of mass of the hot H₂ within a $5.5 \times 10^4 pc^2$ area. The grey-scale is in units of M_{\odot}/pc^2 and also represents the amount of mass of the warm H₂ within a $5.5 \times 10^4 pc^2$ area.

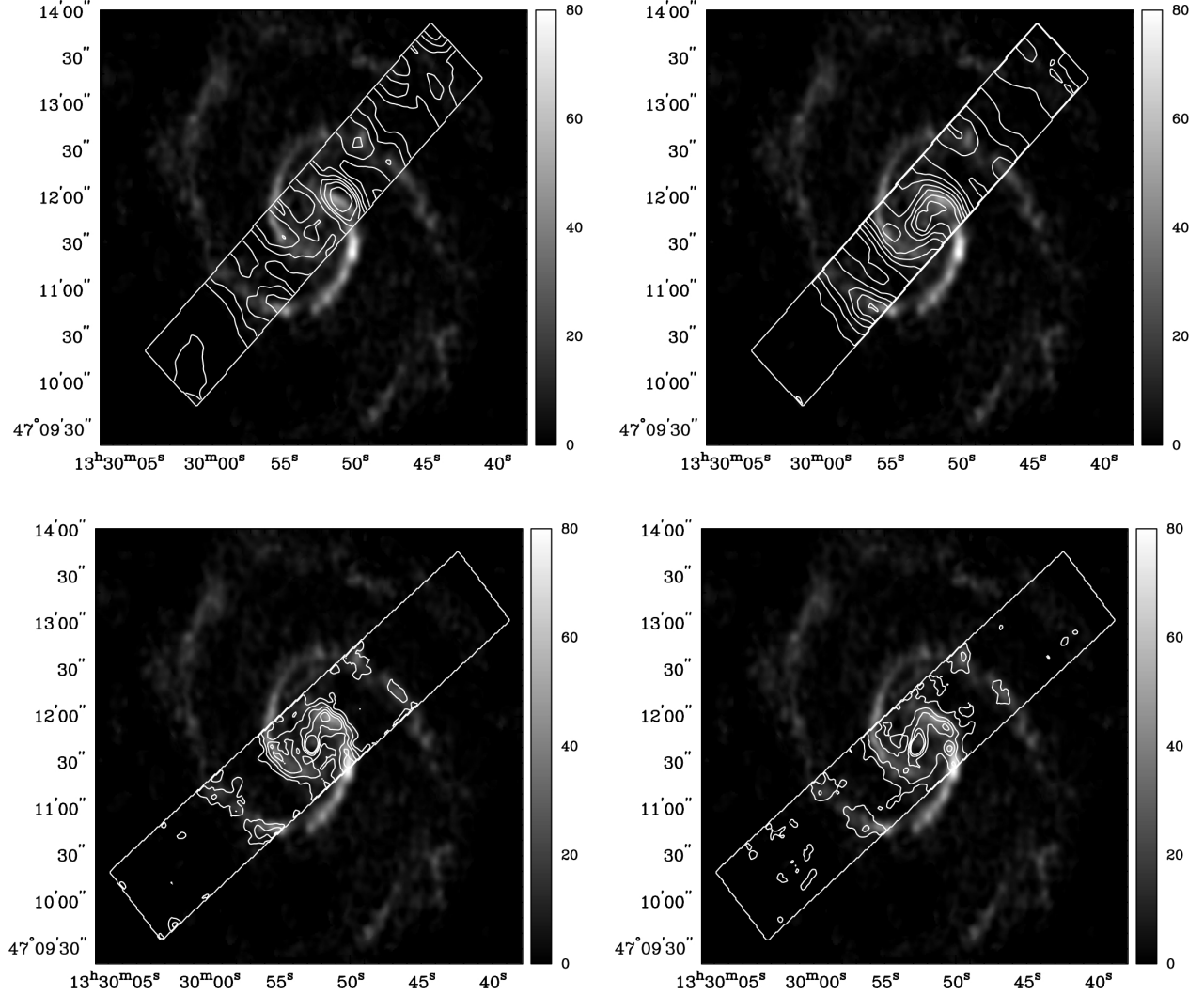


Fig. 6.— Comparison of the CO emission to the H₂ S(0) (top left), H₂ S(1) (top right), H₂ S(2) (bottom left), and H₂ S(3) (bottom right) emission. The CO emission maps are in units of Jy beam s⁻¹. Contour levels for H₂ S(0), H₂ S(1), H₂ S(2), and H₂ S(3) are at the same levels as those used in Figure 1 and Figure 2.

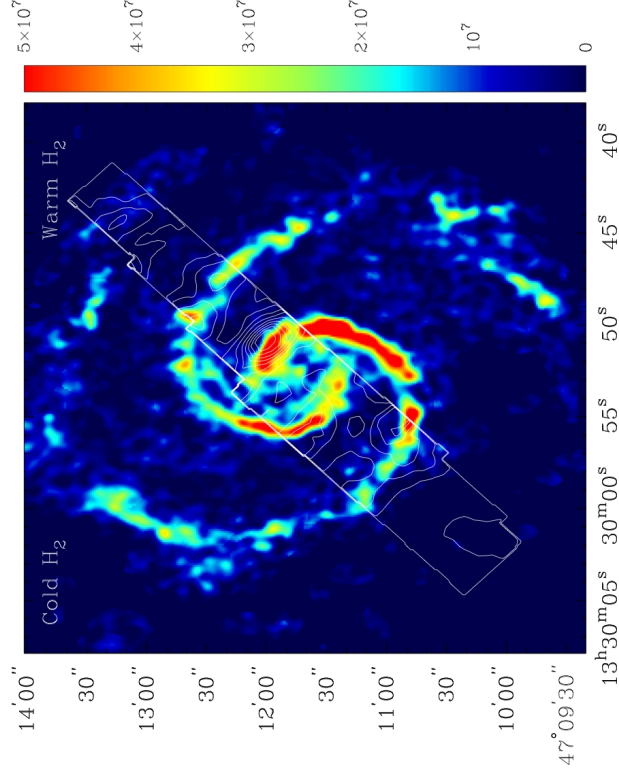


Fig. 7.— Comparison of the cold H₂ (as traced by the CO emission) to the warm (T = 150-275 K) H₂ mass. Cold H₂ mass is in units of M_⊙. Warm H₂ mass contours are the same as in Figure 4.

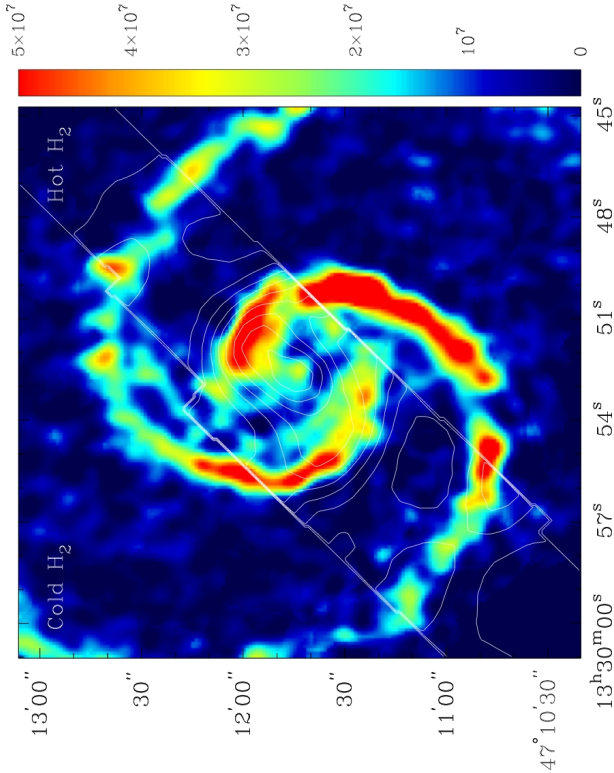


Fig. 8.— Comparison of the cold H₂ (as traced by CO emission) to the hot (T = 500-1000 K) H₂ mass. Cold H₂ mass is in units of M_⊙. Hot H₂ mass contours are the same as in Figure 5.

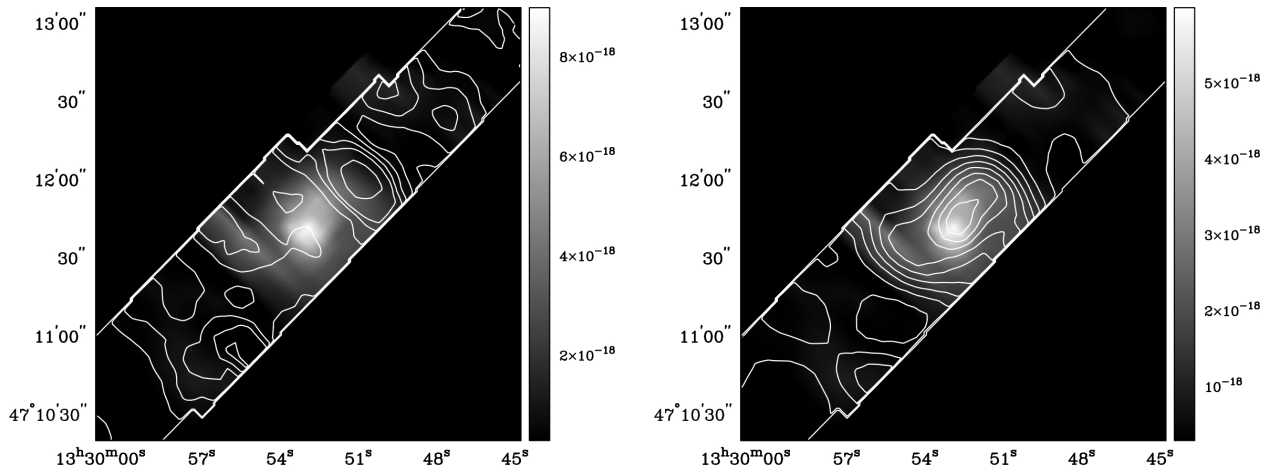


Fig. 9.— *Left:* Comparison of the [OIV](25.89 μm) emission (in grey) to the warm ($T = 175 \text{ K} - 275 \text{ K}$) H₂ mass distribution (in contours). Hot H₂ mass contours are the same as in Figure 4. *Right:* Comparison of the [OIV](25.89 μm) emission (in grey) to the hot ($T = 500 - 1000 \text{ K}$) H₂ mass distribution (in contours). Hot H₂ mass contours are the same as in Figure 5. The [OIV](25.89 μm) emission is in units of W/m².

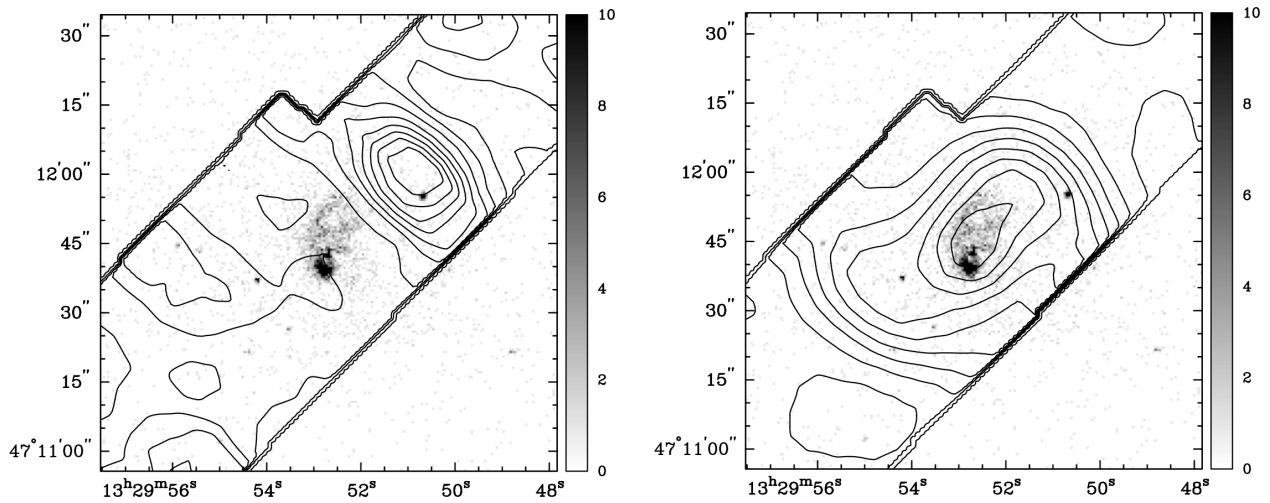


Fig. 10.— *Left:* Comparison of the 0.5 - 10 keV x-ray emission band (in grey) to the warm ($T = 175 - 275$ K) H_2 mass distribution (in contours). X-ray emission is in units of counts. H_2 mass contours are the same as in Figure 4. *Right:* Comparison of the 0.5 - 10 keV x-ray emission band (in grey) to the hot ($T = 500 - 1000$ K) H_2 mass distribution (in contours). The H_2 mass distribution contours are the same as in Figure 5.

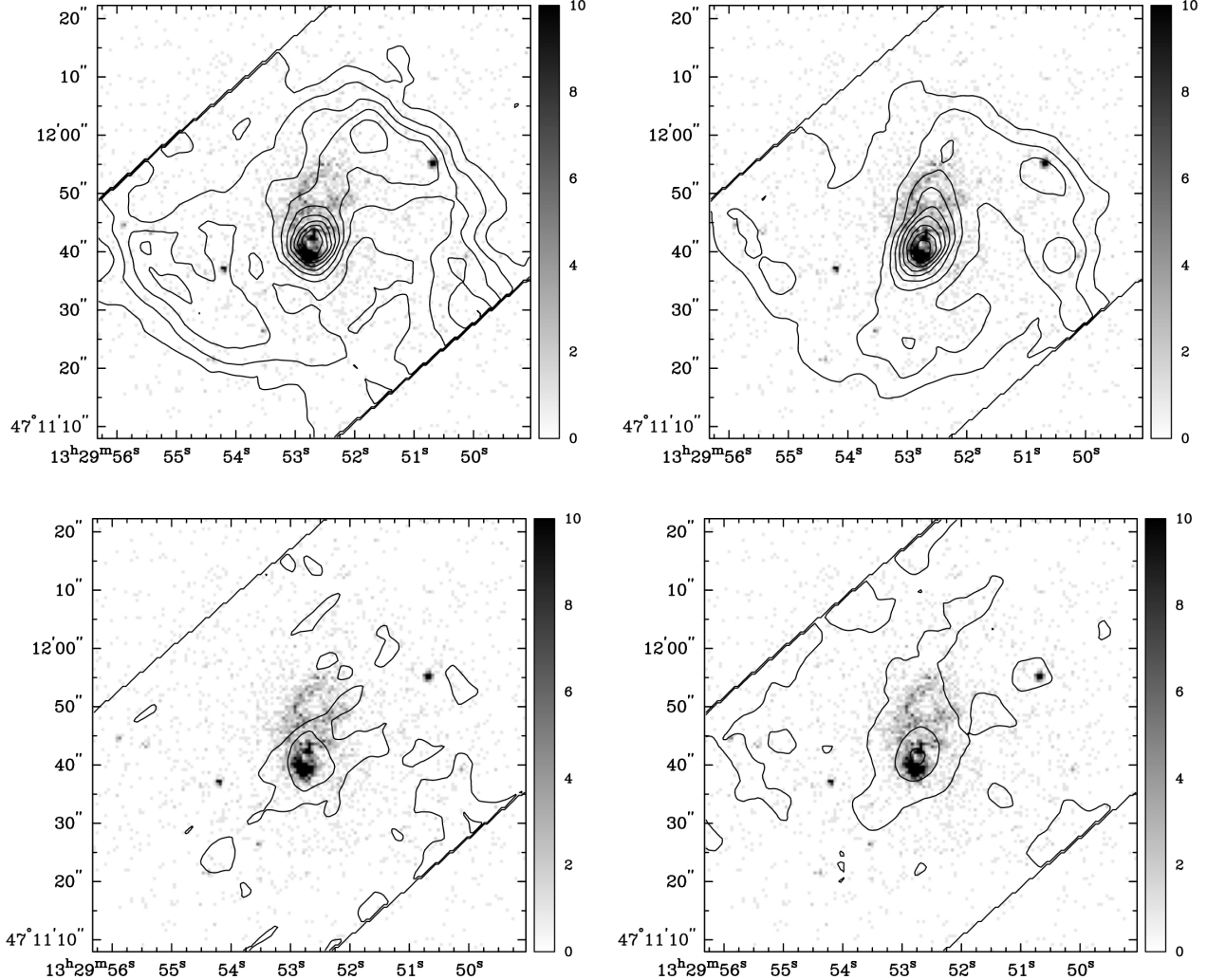


Fig. 11.— Comparison of 0.5 - 10 keV x-ray emission band (in grey) to the H₂ S(2) (top left), H₂ S(3) (top right), H₂ S(4) (bottom left), and H₂ S(5) (bottom right) emission in the nuclear region of NGC 5194. X-ray emission is in units of counts. The H₂ S(2) and H₂ S(3) emission contours are at 10% of their peak values (2.20×10^{-18} and 1.35×10^{-17} W/m², respectively). The H₂ S(4) contours are at 2.0×10^{-18} and 1.0×10^{-18} W/m² and the H₂ S(5) contours are at 7.3×10^{-18} , 4.0×10^{-18} , and 8.0×10^{-19} W/m².

Table 1. H₂ Parameters

| Transition | Wavelength (μm) | Rotational State (J) | Energy (E/k) | A (s^{-1}) | Statistical Weight (g) |
|--------------------------|------------------------------|----------------------|--------------|------------------------|------------------------|
| H ₂ (0-0)S(0) | 28.22 | 2 | 510 | 2.94x10 ⁻¹¹ | 5 |
| H ₂ (0-0)S(1) | 17.04 | 3 | 1015 | 4.76x10 ⁻¹⁰ | 21 |
| H ₂ (0-0)S(2) | 12.28 | 4 | 1682 | 2.76x10 ⁻⁹ | 9 |
| H ₂ (0-0)S(3) | 9.66 | 5 | 2504 | 9.84x10 ⁻⁹ | 33 |
| H ₂ (0-0)S(4) | 8.03 | 6 | 3474 | 2.64x10 ⁻⁸ | 13 |
| H ₂ (0-0)S(5) | 6.91 | 7 | 4586 | 5.88x10 ⁻⁸ | 45 |
| H ₂ (0-0)S(6) | 6.11 | 8 | 5829 | 1.14x10 ⁻⁷ | 17 |
| H ₂ (0-0)S(7) | 5.51 | 9 | 7197 | 2.00x10 ⁻⁷ | 57 |

Note. — The statistical weight (g) is $(2J+1)(2I+1)$ where I equals 1 for odd J transitions (ortho transitions) and I equals 0 for even J transitions (para transitions).

Table 2. Resolution of the H₂ Maps

| Transition | Wavelength (μm) | Spatial Resolution | $\lambda/\delta\lambda$ |
|--------------------------|------------------------------|--------------------|-------------------------|
| H ₂ (0-0)S(0) | 28.22 | 10''.2 | 155 |
| H ₂ (0-0)S(1) | 17.04 | 6''.17 | 185 |
| H ₂ (0-0)S(2) | 12.28 | 4''.37 | 198 |
| H ₂ (0-0)S(3) | 9.66 | 3''.44 | 156 |
| H ₂ (0-0)S(4) | 8.03 | 2''.85 | 129 |
| H ₂ (0-0)S(5) | 6.91 | 2''.46 | 223 |